Quaternary Science Reviews 152 (2016) 72–79

Contents lists available at ScienceDirect

Quaternary Science Reviews

journal homepage: www.elsevier.com/locate/quascirev

Global ice volume during MIS 3 inferred from a sea-level analysis of sedimentary core records in the Yellow River Delta

T. Pico [a, *], J.X. Mitrovica [a], K.L. Ferrier [b], J. Braun [c, d]

[a] Department of Earth and Planetary Sciences, Harvard University, Cambridge, United States
[b] School of Earth and Atmospheric Sciences, Georgia Institute of Technology, Atlanta, United States
[c] ISTerre, Université Grenoble Alpes and CNRS, 38041 Grenoble Cedex 9, France
[d] GFZ Deutsches GeoForschungZentrum, 14473 Potsdam, Germany

ARTICLE INFO

Article history:
Received 10 June 2016
Received in revised form
16 September 2016
Accepted 19 September 2016
Available online 4 October 2016

Keywords:
Glacio isostatic adjustment
MIS 3
Sea level
Sediment
Yellow River Delta

ABSTRACT

Estimates of global ice volume during the glacial phase of the most recent ice age cycle are characterized by significant uncertainty, reflecting the relative paucity of geological constraints on sea level relevant to this time interval. For example, during the middle stages of Marine Isotope Stage 3, published estimates of peak global mean sea level (GMSL) relative to the present range from −25 m to −87 m. The large uncertainty in GMSL at MIS 3 has significant implications for estimates of the rate of ice growth in the period leading to the Last Glacial Maximum (~26 ka). We refine estimates of global ice volume during MIS 3 by employing sediment cores in the Bohai and Yellow Sea that record a migration of the paleo-shoreline at ~50–37 ka through a transition from marine to brackish conditions. In particular, we correct relative sea level at these sites for contamination due to glacial isostatic adjustment using a sea-level calculation that includes a gravitationally self-consistent treatment of sediment redistribution and compaction, and estimate a peak global mean sea level of −38 ± 7 m during the interval 50–37 ka. With suitable sedimentary core records, the approach described herein can be extended to refine existing constraints on global ice volume across the entire glacial period.

1. Introduction

Ice volume variations through the last glacial cycle are a direct and sensitive measure of ice age climate change, and a key input into models of glacial isostatic adjustment (GIA). These variations have been constrained using oxygen isotope records of benthic and planktic foraminifera from deep-sea sedimentary cores (Siddall et al., 2008) and a wide range of geological markers of sea level, including erosional and constructional terraces, sedimentary and biological facies, and coral reefs (Lambeck and Chappell, 2001; Yokoyama et al., 2000; Muhs et al., 2012; Hanebuth et al., 2006). However, the accuracy of ice volume inferences based on oxygen isotope records is limited by regional variability, uncertainties in the conversion from $\delta^{18}O$ related to temperature, and the mean isotopic concentration of continental ice (Siddall et al., 2008; Waelbroeck et al., 2002). Moreover, geological markers of sea-level change are spatially and temporally sparse, and estimates of ice volume based upon them must account for a variety of contaminating signals, most notably GIA (Lambeck and Chappell, 2001; Lambeck et al., 2014; Milne and Mitrovica, 2008). The sparsity of the record is particularly problematic for the period prior to the Last Glacial Maximum (LGM) since many markers of sea level, created during more extensive ice cover, are now submerged. For these reasons, estimates of ice volumes during the bulk of the last glaciation phase, extending from Marine Isotope Stage (MIS) 5c (~100 ka; i. e. Muhs et al., 2012) through MIS 3 (60–25 ka; Siddall et al., 2008), are uncertain to within tens of meters of equivalent global mean sea level (GMSL), where GMSL is defined as the globally averaged sea-level change associated with a given change in total ice mass inventory (i.e., the volume of meltwater divided by the area of the ocean).

Constraints on ice volumes and GMSL during MIS 3 provide an illustrative case in point. Siddall et al. (2008) summarized and compared individual (e.g., Shackleton, 2000) and stacked benthic records (Lisiecki and Raymo, 2005), in addition to planktic records (Dannenmann et al., 2003), during this stage. As an example, over the time period 50–37 ka, peak GMSL estimates can range from −25 to −87 m, relative to present (Siddall et al., 2008). After correcting the coral record at Huon Peninsula for the signal due to GIA and tectonic uplift, Lambeck and Chappell (2001) concluded

* Corresponding author.
E-mail address: tpico@g.harvard.edu (T. Pico).

http://dx.doi.org/10.1016/j.quascirev.2016.09.012
0277-3791/

that GMSL fell from −60 m to −80 m during the same period, while the global ice history model ICE-5G is characterized by a GMSL value within the range −87 m to −100 m across this time interval (Peltier and Fairbanks, 2006). The sea-level lowstand at the Last Glacial Maximum (LGM; 26 ka; Clark et al., 2009) reached ~ −130 m (Yokoyama et al., 2000; Austermann et al., 2013), and therefore, within current uncertainty, global ice volume may have increased by more than a factor of 3 or by less than one-third in the 15 kyr period leading up to the LGM.

In this paper our goal is to refine estimates of global ice volume in the middle of MIS 3, from ~50 to 37 ka, using sedimentary cores from the Yellow River Delta in the Bohai Sea of China. These cores record a transition from marine to freshwater conditions at this time that reflects a migration of the ocean margin across the area and they provide an important constraint on local sea level. We correct the inferred local sea-level history in the region for GIA-induced sea-level change using a numerical model that includes a gravitationally self-consistent treatment of the impact of sediment redistribution (Dalca et al., 2013), and reconstruct GMSL during this time interval. The analysis will explore the sensitivity of the estimate of GMSL to various inputs adopted in the GIA calculation, including the models for sediment redistribution (which incorporates erosion, deposition, and compaction), ice history, and Earth structure.

2. Methods

2.1. GIA modeling

Local sea-level changes are not simply related to fluctuations in global ice volume. Ice sheet growth and melting on a viscoelastic Earth produces a complex spatio-temporal pattern of sea level change that is dependent on the full history of the surface mass (ice, water and sediment) load. The redistribution of surface loads over glacial cycles perturbs the Earth's gravitational field through crustal deformation and direct self-attraction, but the redistribution of water is, in turn, governed by this perturbation since the sea surface must remain a gravitational equipotential in a static sea-level theory. Farrell and Clark (1976) were the first to derive a gravitationally self-consistent sea-level theory – the so-called sea-level equation – under the assumption of a non-rotating Earth with fixed shoreline geometry. Their canonical work has been extended to include the effects of rotation (Milne and Mitrovica, 1996), evolving shorelines associated with local sea level changes and/or the migration of grounded, marine-based ice (Johnston, 1993; Milne et al., 1999; Lambeck et al., 2003; Kendall et al., 2005), and, most recently, sediment redistribution (Dalca et al., 2013). In the present study, we adopt the Dalca et al. (2013) sea-level theory, modified to incorporate sediment compaction, and solve it using the pseudo-spectral algorithm described in that paper. For this purpose we use a spherical harmonic truncation at degree and order 512, which represents a surface spatial resolution of ~40 km.

Relative sea level (SL) is defined as the height of the equipotential that coincides with the ocean surface (G) relative to the elevation of the solid surface:

$$SL = G - (R + H + I), \tag{1}$$

where R is the elevation of the crust, not including sediments and grounded ice, I is the thickness of grounded ice, and H is the thickness of sediment. We will henceforth use the terms “sea level” and “relative sea level” interchangeably. We will be concerned here with perturbations in sea level and each of the components in equation (1) from an initial time t_0 to a time t_j. If we denote this perturbation by the symbol Δ, then we can write:

$$\Delta SL_j = \Delta G_j - (\Delta R_j + \Delta H_j + \Delta I_j). \tag{2}$$

Our sea-level predictions solve for ΔSL_j, ΔG_j and ΔR_j, given time-varying input fields ΔH_j and ΔI_j. We prescribe the sediment redistribution, ΔH_j, as an input field computed from a database of dated sediment cores. Because these sediments have undergone compaction, we define the decompacted sediment thickness H_j at time t_j as

$$H_j = H_{present} - (h_j - \delta_j) \tag{3}$$

where $H_{present}$ is the sediment thickness at present to bedrock, H_j is the sediment thickness at t_j, h_j is the compacted sediment thickness deposited from time t_j to present day, and δ_j is the amount that H_j compacted from t_j to the present (see Fig. 1 for illustration).

$H_{present}$ is obtained from a map of isopach sediment thickness to bedrock, and h_j is determined from dated sedimentary cores. We calculate the elevation difference due to decompaction, δ_j, by using the input fields h_j and $H_{present}$, and by assuming an exponential porosity depth relationship (i.e. Athy, 1930; Guillocheau et al., 2012),

$$\Phi(z) = \Phi_0 e^{-\frac{z}{z_0}} \tag{4}$$

where Φ_0 is the surface porosity, z is depth, and z_0 is a lithology-dependent constant. By equating the sediment grain mass in the sediment column before and after compaction we may derive an expression for δ_j (details included in Appendix A):

$$\delta_j = \frac{\Phi_0 h_j \left(1 - e^{-\frac{H_{present}}{z_0}}\right)}{\left(1 - \Phi_0 e^{-\frac{H_{present}}{z_0}}\right)} \tag{5}$$

As noted above, the thickness of sediment deposited since the initial time step ($j = 0$) to time t_j is:

$$\Delta H_j = H_j - H_0. \tag{6}$$

This value of ΔH_j is the input into Equation (2).

Next, we turn to prescribing the surface mass load. In Dalca et al. (2013), the history of loading is written as

$$\Delta L_j = \rho_w \Delta S_j + \rho_I \Delta I_j + \rho_H \Delta H_j \tag{7}$$

where ρ_w, ρ_I, ρ_H are the (assumed constant) densities of water, ice and sediment, respectively, and ΔS_j is the change in ocean

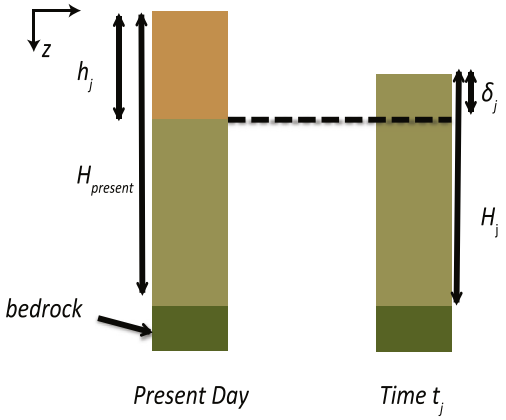

Fig. 1. Schematic illustration of sediment compaction and various parameters discussed in the text.

thickness. However, ρ_H is not uniform when sediment compaction is accounted for. To determine the total bulk sediment load at time step t_j we calculate the average bulk density of the decompacted sediment thickness at t_j ($\overline{\rho}_{H_j}$) and at t_0 ($\overline{\rho}_{H_0}$). Then, in place of Equation (7), we use the expression:

$$\Delta L_j = \rho_w \Delta S_j + \rho_I \Delta I_j + \left(\overline{\rho}_{H_j} H_j - \overline{\rho}_{H_0} H_0\right) \quad (8)$$

In addition, incorporating sediment compaction requires that we track the water storage capacity of the sediment pore space. To conserve total mass, any volume of water incorporated into pore space must be removed from the total ocean volume budget. In this regard, both the additional water volume accommodated into the pore space of newly deposited sediment, and the water volume expulsed from the underlying strata during compaction, must be accounted for. We track a water volume term, W_j, which is equal to the difference between newly created pore space and newly reduced pore space, and incorporate this term in the total water budget to conserve mass (Appendix A).

Finally, the contribution of sediment redistribution to sea level changes includes two components: (1) the perturbation to the crustal height, ΔR_j, and sea surface height, ΔG_j, due to deformation by the sediment load; and (2) the decompacted sediment thickness, ΔH_j, at a given time step, which is comprised of the compacted sediment thickness, h_j, and the elevation difference, δ_j, due to compaction of underlying strata. To calculate the paleotopography, we use values for h_j derived from the constructed regional sediment redistribution model, whereas when citing predictions at the core sites we adopt the value from the core itself (see below).

In the initial simulation discussed below, we adopt the ICE-5G Version 1.2 model of ice history (ΔI) over the last ice age cycle (Peltier, 2004; Peltier and Fairbanks, 2006). The GMSL curve for the ICE-5G model is shown in Fig. 2 (black line). As noted above, the model is characterized by GMSL of −87 m to −100 m during the time period 50–37 ka. ICE-5G is paired with the VM2 model for the radial profile of mantle viscoelastic structure. VM2 is characterized by a lithospheric thickness of 90 km and a mantle viscosity that increases from ~5 × 10^{20} Pa s in the upper mantle to ~3 × 10^{21} Pa s in the deep mantle, and the ICE-5G/VM2 combination is tuned to fit a global database of relative sea level histories (Peltier and Fairbanks, 2006). Following this initial calculation, we will consider a suite of 300 ice histories that sample a wide range of GMSL values through the glaciation phase (Fig. 2); We created each of the alternative ice histories by randomly sampling the range of estimated GMSL values shown by the gray shaded region in Fig. 2; for example, each ice history is constrained to pass through the GMSL range −30 to −80 m at 44 ka (details regarding the construction of these ice histories are provided in the Supplementary Material). We will also consider a set of alternate viscoelastic Earth models.

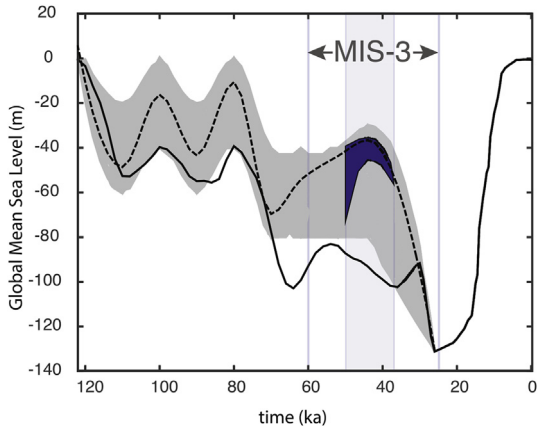

Fig. 2. GMSL change associated with the ICE-5G ice history for the last glacial cycle (solid black line). The shaded region encompasses GMSL of 300 ice histories used in a sensitivity analysis described in the text. The dashed line indicates the ice history adopted in the prediction shown in Fig. 5B. The blue shaded region indicates the full range of GMSL values within the time window 50–37 ka (shaded rectangle) that fit constraints imposed by shoreline indicators, as discussed in the text. The duration of MIS 3 is labeled on the figure. (For interpretation of the references to colour in this figure legend, the reader is referred to the web version of this article.)

2.2. Sediment redistribution models for the Yellow River Delta

We next turn our attention to the construction of a sediment redistribution model (h_j) for the Yellow River Delta region. Sediment loads perturb the predicted sea-level change due to GIA, particularly at sites close to river deltas, where large masses of sediment are deposited in prograding and receding patterns on the continental shelf in response to ice age cycles (Simms et al., 2007; Dalca et al., 2013; Ferrier et al., 2015; Wolstencroft et al., 2014).

The shallow nature of the Bohai Sea, which has a mean depth of 20 m and a maximum depth of 70 m, makes the area highly sensitive to changes in sea level (Fig. 3). Indeed, relatively small changes in local sea level can lead to significant migration of the shoreline and inundation or exposure of large swaths of the continental shelf. Thus, sediment cores in this region have the potential to record shoreline migration in preserved fossils that reflect the brackish or marine environments in which they were deposited. In particular, during the middle stages of MIS 3, three cores (HB-1, SYS-0701, YS01A) contain dated fossils that bound the location of the paleoshoreline (Table 1). Specifically, fossils deposited in core HB-1 are littoral or tidal flat species and dated to cal 42.76–46.96 ka BP (2σ) and cal 41.25–44.02 ka BP (2σ), while fossils in core YS01A are shallow marine and dated to cal 39.76–41.11 ka BP (2σ). Core SYS-0701 contains a gradient of marine to brackish fossils, indicating that the shoreline was close to the core site during MIS 3, with geochronology on a pair of fossils returning ages of cal 46.16–50.00 ka BP (2σ) and cal 44.84–49.50 ka BP (2σ) and a quartz sand near the exposure surface dated by optically stimulated luminescence (OSL) to 41 ± 4 ka (See Supplementary Material for dating and calibration methods).

Radiocarbon dates in the range of 40–50 ka are at the limit of reliability for this dating technique. Samples that return such ages

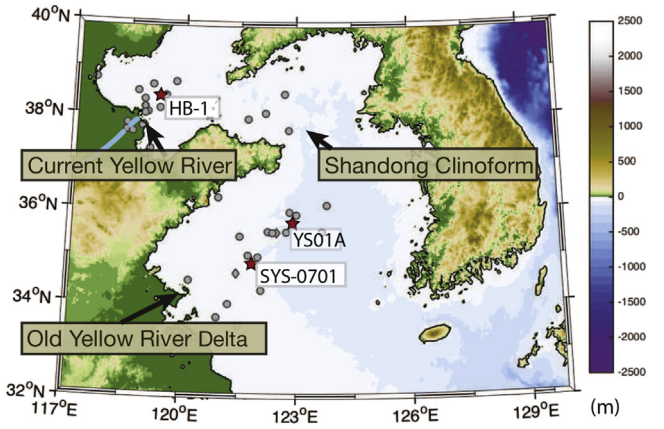

Fig. 3. The location of sedimentary cores used to construct sediment transfer models. During the period 50–37 ka, core HB-1 is characterized by littoral fossils (i.e., a terrestrial environment), YSO1A by marine fossils, and SYS-0701 by a transition from marine to brackish fossils.

Table 1
Geochronological data constraining paleoshoreline location. Ranges for dates derived from ^{14}C are cal ka BP (2σ).

Core name	Core depth (m)	Age (ka)	Dating method	Material dated	Reference
HB-1	35.33	41.25–44.02	^{14}C	gastropod	Liu et al., 2009
HB-1	35.33	42.76–46.96	^{14}C	mollusc shell	Liu et al., 2009
SYS-0701	10.19	41 ± 4	OSL	quartz sand	Liu et al., 2010
SYS-0701	10.70	43 ± 4	OSL	quartz sand	Liu et al., 2010
SYS-0701	15.22	45 ± 5	OSL	quartz sand	Liu et al., 2010
SYS-0701	18.41	46.16–50.00	^{14}C	mollusc shell	Liu et al., 2010
SYS-0701	20.30	44.84–49.50	^{14}C	mollusc shell	Liu et al., 2010
SYS-0701	22.96	48 ± 5	OSL	quartz sand	Liu et al., 2010
YS01A	28.65	39.76–41.1	^{14}C	foraminifera	Wang et al., 2014

may be older, and reflect contamination that would cause a radiocarbon-dead sample to give a date in this range. However, four OSL dates in this core span 41 ± 4 ka to 48 ± 5 ka from a depth of 10.19–22.95 m (i.e., they bound radiocarbon dates stratigraphically), and these add confidence to the radiocarbon dates. Considering the error on these dates the shoreline could have been located at this site at any point during the period 50 to 37 ka. In the results below, we will display shoreline reconstructions in the middle of this interval, at 44 ka.

We constructed three different models for sediment redistribution in the region using 49 well-dated sediment cores (see Fig. 3 for site locations) and river flux measurements in both the drainage area upstream of the Yellow River Delta and within depositional environments in the Bohai and Yellow Sea (see Supplementary Material for core database details). On-land erosion and deposition rates are calculated using river flux measurements, and erosion rates are assigned uniformly within each of six sub-basins. Accumulation rates on the continental shelf are calculated using radiocarbon or optically dated surfaces in the cores. These rates of erosion and deposition are assigned to grids with spacing consistent with our spherical harmonic truncation at degree 512, and these grids are constructed at time steps spanning the last glacial cycle.

Sediment deposition in the region occurred in three depocenters as the river mouth avulsed between the current and old river deltas, and as ocean currents transported sediment around the Shandong peninsula. We label these depocenters as the current delta, old delta, and Shandong Clinoform. To create maps of sediment redistribution we adopt three different methods to interpolate between local accumulation rate estimates at core sites (Fig. 4).

In Scheme 1 (Fig. 4a), linear interpolation is employed between all core-based estimates. Because core data is sparse, and generally does not sample areas in between depocenters, Scheme 1 is likely to assign higher than actual sedimentation rates in areas outside of depocenters that are known to have low accumulation rates. Similarly, because cores do not sample the entire depocenter region, it is possible that accumulation within the depocenter is underestimated using simple interpolation. Scheme 2 (Fig. 4b) avoids this bias by applying a linear interpolation between cores located within each of the three depocenters. However, similar to Scheme 1, this scheme also likely underestimates the amount of sediment in depocenters. Finally, in Scheme 3 (Fig. 4c), we assign to each depocenter a uniform accumulation rate equal to the average rate in sediment cores that fall within the area. This scheme provides a more realistic representation of the total sediment load in depocenters, but it does not account for both the potentially large geographic variability in accumulation rates within each depocenter and the evolution in the areal extent of depocenters through time.

Fig. 4d shows our model of the accumulated thickness of terrestrial erosion and deposition based on present-day river flux measurements. Our sea-level simulations must conserve mass; thus the amount of sediment eroded must equal the amount deposited. As an example, consider the last 1000 years. We assume that erosion rates, and hence deposition rates, are similar to modern values as this time period reflects the anthropogenic influence of agriculture in the region (i.e. Milliman et al., 1987; Mei-E and Xianmo, 1995). However, the reconstructed volume of erosion over the past 1000 years was higher than the volume of sediment deposition estimated from the core records over that period. The ratio between total eroded and deposited volume is 1.32, 5.02, and 3.09, respectively for Schemes 1, 2, and 3. To preserve the deposition volumes recorded in the sediment cores, we choose to scale erosion rates down to match the depositional record. During earlier periods such as MIS 3, where erosion rates are not constrained, we apply the same methodology; that is, we apply a unique scaling factor to each time step to conserve mass. In this process we preserve the relative contribution of each drainage sub-basin shown in Fig. 4d. This yields a time history of erosion and deposition covering the last glacial cycle.

As a final point, we note that the three sediment models discussed above are used to define the sediment load component of the total surface mass load (equation (8)) which is necessary for the calculation of the load-induced crustal deformation and sea surface perturbation (ΔR and ΔG, respectively, in equation (2)). As noted above, whenever we cite sea-level results at the three core sites HB-1, YS01A and SYS-0701 (Fig. 3), we use the sediment thickness of the dated core, rather than that of the sediment redistribution model, to compute the change in topography associated with sediment height (ΔH_j in equation (2)).

3. Results

We will begin by considering results based on Scheme 3 (Fig. 4c). We consider interpolation Scheme 3 to be the most realistic model of sediment deposition in the basin since the sediments are only distributed within known areas of deposition.

We ran two ice age sea level simulations adopting the ICE-5G ice history coupled to the VM2 Earth model, one including and the other not including sediment redistribution. Fig. 5a shows the predicted positions of the shoreline at 44 ka for these two cases. As previously noted, the fossil record at core SYS-0701 indicates that the paleoshoreline was close to the site from 50 to 37 ka. In contrast, the ICE-5G/VM2 predictions place the site well away from the paleoshoreline and at an elevation of either 44.0 m in the case when sediment redistribution is included, or 53.7 m for calculations that do not include the loading effect of the sediment redistribution or its compaction through time. In this regard at the site SYS-0701, our compaction model yields an estimate of δ_j of 8.04 m, based on the lithology, isopach thickness, and compacted sediment thickness accumulated since 44 ka (Fig. 1).

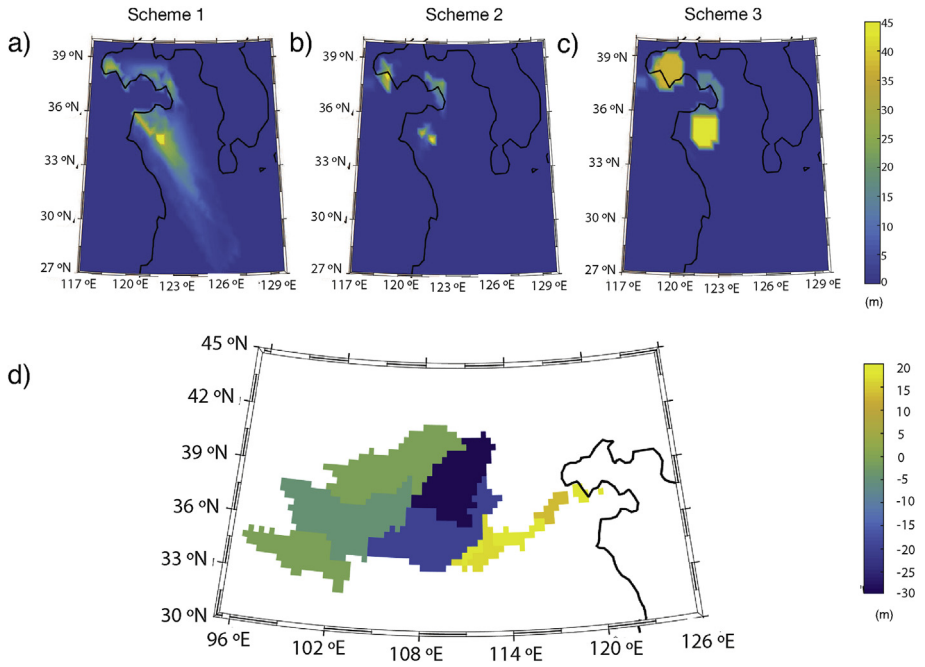

Fig. 4. (a–c) Regional sediment redistribution models constructed using three interpolation schemes. a) Scheme 1: Linear interpolation between all core accumulation rates in Fig. 3 b) Scheme 2: Linear interpolation within each depocenter region (current delta, old delta, and clinoform) individually. c) Scheme 3: Average depocenter accumulation rate is assigned uniformly in space across each depocenter. d) On-land erosion and deposition, based on present-day measurements. All frames show accumulated thicknesses over the last glacial cycle.

The simulation shown in Fig. 5a suggests that in order to match paleoshoreline data, relative sea level must have been ~45 m higher at 50–37 ka than the value predicted by ICE-5G. This mismatch is substantial, and suggests a significant discrepancy between the true global ice volume and that of the ICE-5G history. To quantify this issue, we ran a large series of simulations that used the same Earth model (VM2) and sediment redistribution model as in Fig. 5a, and were distinguished on the basis of the adopted ice history.

We predicted the shoreline location and the elevation of the core site SYS-0701 at 44 ka using the full suite of ice histories associated with the GMSL curves bounded by the shaded region in Fig. 2. We then retained from this set of simulations only those results that predicted shoreline locations that: (1) were consistent with the geological settings (marine, brackish, or terrestrial) imposed by the cores YS01A, SYS-0701, and HB-1, respectively; and (2) predicted an elevation of site SYS-0701 at 44 ka within the range −3 m to 3 m, the local tidal range which bounds possible elevations for brackish deposition (as in Yokoyama et al., 2000). In Fig. 6 we show the distribution of GMSL values associated with the subset of 46 simulations that satisfied these constraints (blue). These GMSL values range from −35.4 m to −45.5 m, (the 46 simulations have a mean of −40.0 m and a standard deviation of 2.6 m). The uncertainty reflects the sensitivity of the inference to possible errors in the ice history across the period from the LIG to MIS 3.

As an example, Fig. 5B shows the reconstructed location of the shoreline predicted by the simulation in which GMSL during MIS 3 was raised by ~50 m relative to the ICE-5G history, corresponding to a GMSL value of −36 m at 44 ka (black dotted line, Fig. 2). In this case, the prediction that includes the impact of sediment redistribution accurately reconstructs the paleoshoreline close to the core site SYS-0701; the predicted elevation of the site at this time is −0.14 m. Moreover, the same prediction places core HB-1 landward of the shoreline and YS01A core in a marine setting at this time, consistent with the fossil records at these sites.

We next considered the sensitivity of these calculations to variations in the sediment history and Earth structure. To begin, we ran simulations in which we adopted the remaining two sediment redistribution models described in the Methods (Fig. 4). We predict elevations of −0.2864, −1.7327, −0.1365 for the three sediment redistribution models (Schemes 1–3, respectively) at 44 ka at the core site SYS-0701. As in Fig. 5B these were all computed using the GMSL history shown by the dotted black line in Fig. 2, and the VM2 Earth model. The differences between the three models (~1.6 m) thus provide a measure of the sensitivity of the predictions to uncertainties in this loading effect.

To quantify the sensitivity to the chosen Earth model we ran a series of simulations using the same 300 ice histories, where the viscosity model VM2 was replaced by two alternate Earth models distinguished by the adopted lithospheric thickness and uniform upper and lower mantle viscosities: (1) 71 km, and 5×10^{20} Pa s and 10^{22} Pa s, consistent with several independent studies of GIA data sets (e.g., Lambeck et al., 1998; Mitrovica and Forte, 2004); and (2) 41 km, and 2×10^{20} Pa s and 5×10^{21} Pa s (consistent with the low-viscosity solution of Lambeck et al., 2014). (we refer to these as Alternate models 1 and 2, respectively.) These choices were guided, in part, by a recent analysis of Holocene relative sea level data in China which suggests that a lower mantle viscosity in excess of $5–10 \times 10^{21}$ Pa s is unlikely for this region (Bradley et al., 2016). The distribution of GMSL values that fall within the required elevation bounds for simulations based on the two alternate Earth models is shown in Fig. 6 (red and yellow bars). The mean values of these distributions are −34.2 m (standard deviation of 1.9 m) and −38.5 m (standard deviation of 2.4 m), for Alternate models 1 and 2, respectively. Accounting for the variability associated with the ice history and Earth model (Fig. 6), and sediment redistribution (−1.6 m), we infer a two sigma bound on peak GMSL in the interval 50–37 ka of -38 ± 7 m. (As we noted above, while the numerical predictions focus on the time 44 ka, errors in the timing of the shoreline migration suggest that the estimated GMSL value was obtained somewhere in the time range 50–37 ka.)

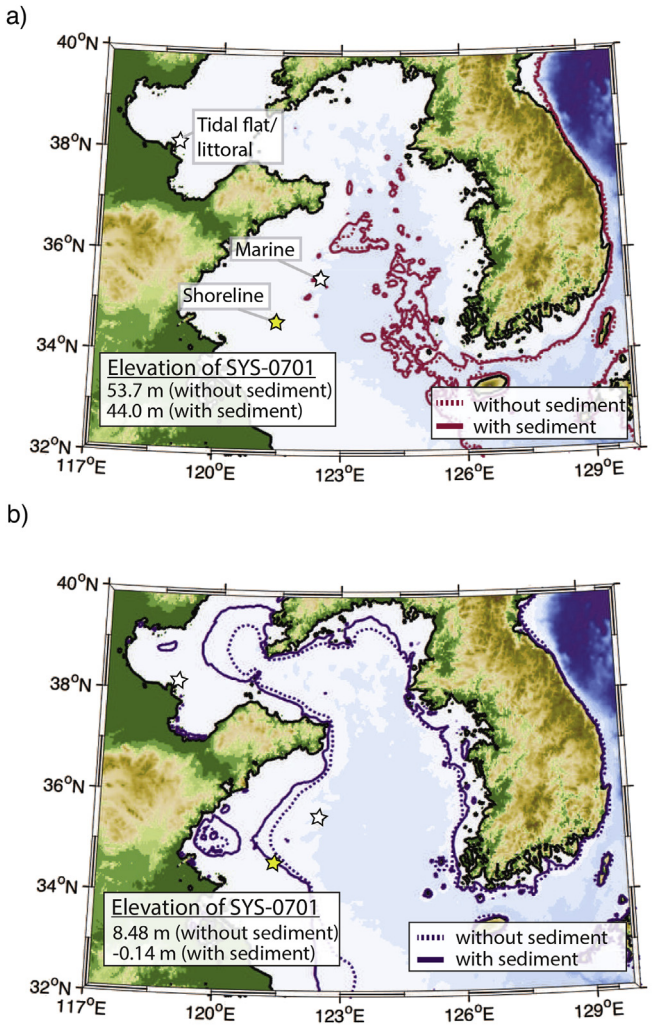

Fig. 5. Predicted shoreline positions at 44 ka. a) Calculations based on the ICE-5G model of ice history and the VM2 viscosity profile, including (solid) and not including (dotted) sediment redistribution. The predicted elevations of the SYS-0701 core site for these simulations are 44.0 m and 53.7 m above the sea surface, respectively. The white stars label cores HB-1 and YS01A, indicating tidal-flat/littoral and marine species, respectively. The yellow star indicates the location of core SYS-0701. b) As in frame (a), except that the ice history is revised to yield the GMSL curve shown by the dotted black line in Fig. 2. In this case, the predicted elevations of the SYS-0701 core site at 44 ka are −0.14 m and 8.48 m, respectively, for simulations with and without sediment redistribution. Details of the sediment redistribution (Scheme 3) are provided in the Methods. (For interpretation of the references to colour in this figure legend, the reader is referred to the web version of this article.)

In Fig. 7 our estimate of −38 ± 7 m for peak GMSL across the period 50–37 ka is compared with inferences from previous studies. The bounds shown for each study represent the minimum and maximum GMSL values inferred over this time interval, and the latter should be compared with our bound on peak GMSL. Our result lies at the upper range of GMSL estimates (minimum ice volume).

4. Conclusions

Constraining ice volumes across the last glacial cycle is an important step toward a deeper understanding of ice age climate and the associated stability of ice sheets. Combining gravitationally self-consistent predictions of GIA-induced sea-level changes that accurately incorporate the effects of sediment redistribution in areas of high deposition and erosion, with dated sedimentary cores

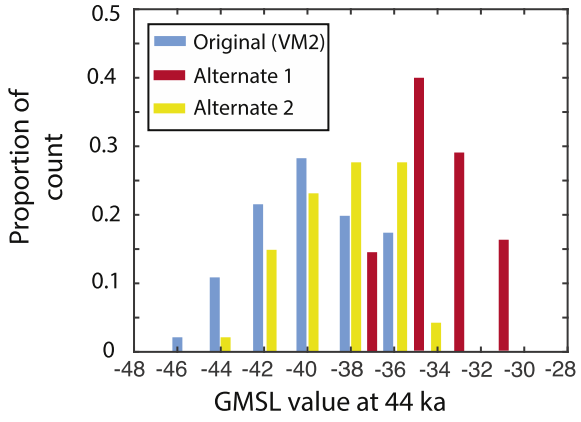

Fig. 6. Distribution of GMSL values at 44 ka for simulations that predict elevations within ±3 m elevation at SYS-0701. Results are shown for Earth model VM2 (blue; values range from −35.4 to −45.5 m, with a population mean of −40.0, a standard deviation of 2.6 m, and a median of −40.0 m); Alternate model 1 (red; −30.1 to −38.0, with a population mean of −34.2, a standard deviation of 1.9 m, and a median of −34.4 m); and Alternate model 2 (yellow; −34.4 to −43.4, with a population mean of −38.5, a standard deviation of 2.4, and a median of −38.0 m). The three viscosity models yield 46, 55, and 47 runs (out of 300 each), respectively, that satisfy the bound at SYS-0701. (For interpretation of the references to colour in this figure legend, the reader is referred to the web version of this article.)

that record transitions from marine to terrestrial environments, provides a novel approach to refining existing estimates of ice volumes during the last glacial phase. We have applied this approach to estimate GMSL in the middle of Marine Isotope Stage 3, 50–37 ka, using core records in the Bohai and Yellow Sea. We conclude that peak GMSL during this time interval was in the range −38 ± 7 m, which indicates that excess (relative to present day) ice volumes increased by a factor of three in the 15 kyr period leading to LGM. In Fig. 7 we compare this bound on GMSL to independent estimates based on mapping oxygen isotope records to global ice volumes (Waelbroeck et al., 2002; Pahnke et al., 2003;

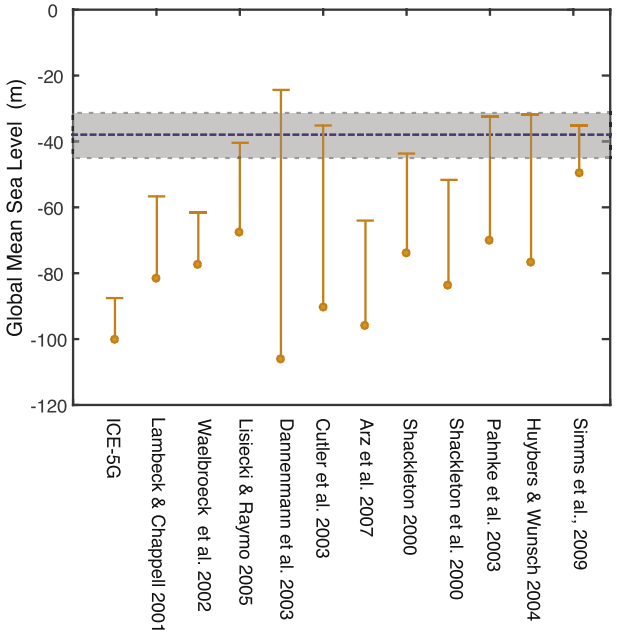

Fig. 7. Estimate of peak GMSL from this study (dotted-line, shading represents the error bound) during the period 50–37 ka. Vertical lines show inferences of maximum and minimum GMSL values from previous, independent analyses (as labeled on the abscissa) summarized in Siddall et al. (2008). The bar on each is to be compared with our new inference of peak GMSL.

Shackleton, 2000; Lisiecki and Raymo, 2005; Dannerman et al., 2003, Cutler et al., 2003; Huybers and Wunsch, 2004; Shackleton et al., 2000, Arz et al., 2007; Simms et al., 2009) or on the sea level record at Huon Peninsula (Lambeck and Chappell, 2001). Of the eleven inferences shown on the figure, the peak GMSL from six of these studies overlap with our revised estimate of GMSL.

Yokoyama et al. (2000) similarly used sea-level indicators in sediment cores, corrected for GIA, in an area of relatively low sedimentation (Bonaparte Gulf, Australia) to estimate a stable GMSL of −135 m at the LGM. With suitable well-resolved and accurately dated sedimentary core records, the approach used herein can be applied across the entire period extending from the end of MIS 5e to the LGM.

Finally, beyond global considerations of Earth system evolution during the last glacial phase, our results also have important implications for studies of local sea level in the Bohai and Yellow Sea regions. In particular, our reconstruction of shoreline evolution, consistent with available core records, provides a key input into studies of human migration patterns in the region (D'Alpoim Guedes et al., 2016).

Acknowledgements

TP was supported by NSF-GRFP and Harvard University. JXM was funded by Harvard University. KLF was supported by NSF grant EAR-1525922.

Appendix A. Supplementary data

Supplementary data related to this article can be found at http://dx.doi.org/10.1016/j.quascirev.2016.09.012.

Appendix

A Sediment compaction

To estimate the effect of compaction on our paleo-topography elevations, we assume a porosity profile that follows an exponential porosity-depth relationship (Athy, 1930):

$$\Phi(z) = \Phi_0 e^{-\frac{z}{z_0}}$$

where Φ_0 is the surface porosity, z is the depth, and z_0 controls the length scale of the porosity reduction with depth.

Consider the two columns in Fig. 8: the one at left pertains to the present day and the other to an arbitrary time in the past, t_j. At present day there is a thickness of sediment h that has accumulated since the time of interest t_j, and a thickness of sediment beneath this to the bedrock, $L'=H_{present}-h_j$. At the time t_j, there is a thickness H_j of sediments to bedrock. The difference H_j-L' is denoted as δ_j. A general expression for volume in a core from the top of the sediment downward at time t_j is:

$$Volume = A\int_0^{H_j}(1-\Phi(z))\mathrm{d}z$$

where A is the cross-sectional area of the column.

The mass of sediment grains in the column H_j and column L' must be equal, and since we assume that the grain density remains constant over time, we can equate the volumes in these two columns. This yields:

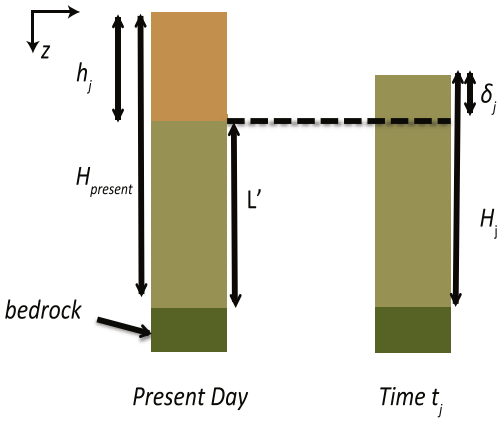

Fig. 8. Schematic illustration of sediment compaction and various parameters discussed in the text. The depth, z, is defined to be 0 at the surface and it increases downward in the column.

$$A\int_0^{H_j}(1-\Phi(z))\mathrm{d}z = A\int_0^{L'+h_j}(1-\Phi(z))\mathrm{d}z - A\int_0^{h_j}(1-\Phi(z))\mathrm{d}z$$

$$\int_0^{H_j}(1-\Phi(z))\mathrm{d}z = \int_0^{h_j}(1-\Phi(z))\mathrm{d}z + \int_h^{L'+h_j}(1-\Phi(z))\mathrm{d}z - \int_0^{h_j}(1-\Phi(z))\mathrm{d}z$$

$$\int_0^{H_j}(1-\Phi(z))\mathrm{d}z = \int_{h_j}^{L'+h_j}(1-\Phi(z))\mathrm{d}z$$

If we substitute $\delta_j=H_j-L'$, we obtain an expression for δ:

$$\delta_j = \Phi_0 z_0\left[1 - e^{-\frac{L'}{z_0}}\left(e^{-\frac{\delta_j}{z_0}} - e^{-\frac{h_j}{z_0}}\right) - e^{-\frac{h_j}{z_0}}\right]$$

Assuming that both δ_j and $h_j \ll z_0$, we can approximate this as

$$\delta_j = \frac{\Phi_0 h_j\left(1 - e^{-\frac{L'}{z_0}}\right)}{\left(1 - \Phi_0 e^{-\frac{L'}{z_0}}\right)}$$

To illustrate how we estimated δ_j, it will help to consider the procedure for decompaction at a single sediment core, SYS-0701. For this purpose, we choose the following values: $\Phi_0 = 0.63$, the surface porosity (Guillocheau et al., 2012); $Z_0 = 3.7$ km, appropriate for clay (Guillocheau et al., 2012); $h_j = 19.3$ m, the average thickness of the core between dates cal 46.97 ka BP and cal 48.48 ka BP, Liu et al., 2010); and $H_{present} = 1.68$ km, the total thickness of the sediment column (Divins, 2003). From these values we estimate a compaction δ_j of 8.04 m for this site. In a similar manner, we can calculate δ_j over the entire region of study by using the sediment thickness h_j from the sediment redistribution models and a map of isopach sediment thickness to bedrock (Divins, 2003).

Sediment loads are calculated according to the equation:

$$\Delta L_j = \rho_w \Delta S_j + \rho_I \Delta I_j + \left(\overline{\rho}_{Hj} H_j - \overline{\rho}_{H0} H_0\right)$$

where the average bulk sediment density $\overline{\rho}_H$ over a given depth is based on the average porosity, $\overline{\Phi}(z)$, such that

$$\overline{\rho}_H = \rho_s - (\rho_s - \rho_w)\overline{\Phi}(z)$$

And $\overline{\Phi}(z)$ is defined as

$$\overline{\Phi}(z) = \frac{1}{z_2 - z_1}\int_{z_1}^{z_2}\Phi(z) = \frac{z_0\Phi_0\left(e^{-\frac{z_1}{z_0}} - e^{-\frac{z_2}{z_0}}\right)}{z_2 - z_1}$$

This can be written as the integral from depth 0 to H_j:

$$\overline{\Phi}(z) = \frac{1}{H_j}\int_{0}^{H_j}\Phi(z) = \frac{-\Phi_0 z_0\left(e^{-\frac{H_j}{z_0}} - 1\right)}{H_j}$$

If we substitute this expression into our equation for average density we obtain:

$$\overline{\rho}_{H_j} = \rho_s + (\rho_s - \rho_w)\frac{\Phi_0 z_0\left(e^{-\frac{H_j}{z_0}} - 1\right)}{H_j}$$

Finally, the water volume storage capacity term is equal to the difference between newly created pore space and newly reduced pore space:

$$W_j = \int_{0}^{H_j}\Phi(z)\mathrm{d}z - \int_{0}^{H_0}\Phi(z)\mathrm{d}z$$

References

Arz, H.W., Lamy, F., Ganopolski, A., Nowaczyk, N., Ptzold, J., 2007. Dominant Northern Hemisphere climate control over millennial-scale glacial sea-level variability. Quat. Sci. Rev. 26 (3–4), 312–321.

Athy, L.F., 1930. Density, porosity, and compaction of sedimentary rocks. AAPG Bull. 14 (1), 194–200. http://dx.doi.org/10.1306/3D93289E-16B1-11D7-8645000102C1865D.

Austermann, J., Mitrovica, J.X., Latychev, K., Milne, G.A., 2013. Barbados-based estimate of ice volume at Last Glacial Maximum affected by subducted plate. Nat. Geosci. 6 (7), 553–557.

Bradley, S.L., Milne, G.A., Horton, B.P., Zong, Y., 2016. Modelling sea level data from China and Malay-Thailand to estimate Holocene ice-volume equivalent sea level change. Quat. Sci. Rev. 137, 54–68. http://dx.doi.org/10.1016/j.quascirev.2016.02.002.

Clark, P., Dyke, A., Shakun, J., Carlson, A., Clark, J., Wohlfarth, B., Mitrovica, J., Hostetler, S., McCabe, M., 2009. The last glacial maximum. Science 325 (5941), 710–714.

Cutler, K.B., Edwards, R.L., Taylor, F.W., Cheng, H., Adkins, J., Gallup, C.D., Cutler, P.M., Burr, G.S., Bloom, A.L., 2003. Rapid sea-level fall and deep-ocean temperature change since the last interglacial period. Earth Planet. Sci. Lett. 206 (3–4), 253–271.

D'Alpoim Guedes, J., Austermann, J., Mitrovica, J.X., 2016. Lost foraging opportunities for East Asian hunter-gatherers due to rising sea level since the last glacial maximum. Archaeolog. Record 0, 1–12. http://dx.doi.org/10.1002/gea.21542.

Dalca, A.V., Ferrier, K.L., Mitrovica, J.X., Perron, J.T., Milne, G.A., Creveling, J.R., 2013. On postglacial sea level—III. Incorporating sediment redistribution. Geophys. J. Int. 194 (1), 45–60.

Dannenmann, S., Linsley, B.K., Oppo, D.W., Rosenthal, Y., Beaufort, L., 2003. East Asian monsoon forcing of suborbital variability in the Sulu sea during marine isotope stage 3: link to northern Hemisphere climate. Geochem. Geophys. Geosys. 4 (1).

Divins, D.L., 2003. Total Sediment Thickness of the World's Oceans & Marginal Seas. NOAA National Geophysical Data Center, Boulder, CO.

Farrell, W.E., Clark, J.A., 1976. On postglacial sea level. Geophys. J. Int. 647–667.

Ferrier, K.L., Mitrovica, J.X., Giosan, L., Clift, P.D., 2015. Sea-level responses to erosion and deposition of sediment in the Indus River basin and the Arabian Sea. Earth Planet. Sci. Lett. 416, 12–20.

Guillocheau, F., Rouby, D., Robin, C., Helm, C., Rolland, N., Le Carlier de Veslud, C., Braun, J., 2012. Quantification and causes of the terrigenous sediment budget at the scale of a continental margin: a new method applied to the Namibia-South Africa margin. Basin Res. 24 (1), 3–30.

Hanebuth, T.J.J., Saito, Y., Tanabe, S., Vu, Q.L., Ngo, Q.T., 2006. Sea levels during late marine isotope stage 3 (or older?) reported from the Red River delta (northern Vietnam) and adjacent regions. Quat. Int. 145–146, 119–134.

Huybers, P., Wunsch, C., 2004. A depth-derived Pleistocene age model: uncertainty estimates, sedimentation variability, and nonlinear climate change. Paleoceanography 19 (1).

Johnston, P., 1993. The effect of spatially non-uniform water loads on prediction of sea-level change. Geophys. J. Int. 114 (3), 615–634.

Kendall, R.A., Mitrovica, J.X., Milne, G.A., 2005. On post-glacial sea level - II. Numerical formulation and comparative results on spherically symmetric models. Geophys. J. Int. 161 (3), 679–706.

Lambeck, K., Smither, C., Johnston, P., 1998. Sea level change, glacial rebound and mantle viscosity for northern Europe. Geophys. J. Int. 134, 102–144.

Lambeck, K., Chappell, J., 2001. Sea level change through the last glacial cycle. Sci. (New York, N.Y.) 292 (5517), 679–686.

Lambeck, K., Purcell, A., Johnston, P., Nakada, M., Yokoyama, Y., 2003. Water-load definition in the glacio-hydro-isostatic sea-level equation. Quat. Sci. Rev. 22 (2–4), 309–318.

Lambeck, K., Rouby, H., Purcell, A., Sun, Y., Sambridge, M., Bard, E., Clark, P.U., 2014. Sea level and global ice volumes from the last glacial maximum to the Holocene, 111 (43), 15296–15303.

Lisiecki, L.E., Raymo, M.E., 2005. A Pliocene-Pleistocene stack of 57 globally distributed benthic δ^{18} O records. Paleoceanography 20 (1), 117.

Liu, J., Saito, Y., Kong, X., Wang, H., Wen, C., Yang, Z., Nakashima, R., 2010. Delta development and channel incision during marine isotope stages 3 and 2 in the western South Yellow Sea. Mar. Geol. 278 (1–4), 5476.

Liu, J., Saito, Y., Wang, H., Zhou, L., Yang, Z., 2009. Stratigraphic development during the late pleistocene and Holocene offshore of the Yellow River delta, Bohai sea. J. Asian Earth Sci. 36 (4–5), 318–331.

Mei-E, Ren, Xianmo, Z., 1995. Anthropogenic influences on changes in the sediment load of the Yellow River. Res. Soil Water Conserv. 2 (4).

Milliman, J.D., Yun-Shan, Q., Mei-E, R., Saito, Y., 1987. Mans influence on the erosion and transport of sediment by Asian rivers: the Yellow River (Huanghe) example. J. Geol. 95 (6), 751–762. http://dx.doi.org/10.1086/629175.

Milne, G.A., Mitrovica, J.X., 1996. Postglacial sea-level change on a rotating Earth: first results from a gravitationally self-consistent sea-level equation. Geophys. J. Int. 126 (3), F13F20.

Milne, G.A., Mitrovica, J.X., 2008. Searching for eustasy in deglacial sea-level histories. Quat. Sci. Rev. 27 (25–26), 2292–2302.

Milne, G.A., Mitrovica, J.X., Davis, J.L., 1999. Near-field hydro-isostasy: the implementation of a revised sea-level equation. Geophys. J. Int. 139, 464–482.

Mitrovica, J.X., Forte, A.M., 2004. A new inference of mantle viscosity based upon a joint inversion of convection and glacial isostatic adjustment data. Earth Planet. Sci. Lett. 225, 177–189.

Muhs, D.R., Simmons, K.R., Schumann, R.R., Groves, L.T., Mitrovica, J.X., Laurel, D., 2012. Sea-level history during the Last Interglacial complex on San Nicolas Island, California: implications for glacial isostatic adjustment processes, paleozoogeography and tectonics. Quat. Sci. Rev. 37, 1–25.

Pahnke, K., Zahn, R., Elderfield, H., Schulz, M., 2003. 340,000-Year centennial-scale marine record of southern Hemisphere climatic oscillation. Science 16 (1), 101108.

Peltier, W.R., 2004. Global glacial isostasy and the surface of the ice-age Earth : the ICE-5G (VM2) Model and GRACE. Annu. Rev. Earth Planet. Sci. 32 (1), 111–149.

Peltier, W.R., Fairbanks, R.G., 2006. Global glacial ice volume and Last Glacial Maximum duration from an extended Barbados sea level record. Quat. Sci. Rev. 25 (23–24), 3322–3337.

Shackleton, N.J., 2000. The 100,000-Year ice-age cycle identified and found to lag temperature, carbon dioxide, and orbital eccentricity. Science 289 (5486), 1897–1902.

Shackleton, N.J., Hall, M.A., Vincent, E., 2000. Phase relationships between millennial-scale events 64,000-24,000 years ago. Paleoceanography 15 (6), 565–569.

Siddall, M., Rohling, E.J., Thompson, W.G., Waelbroeck, C., 2008. Marine Isotope Stage 3 sea level fluctuations: data synthesis and new outlook. Hemisphere 46 (2007), 1–29.

Simms, A.R., Lambeck, K., Purcell, A., Anderson, J.B., Rodriguez, A.B., 2007. Sea-level history of the Gulf of Mexico since the last glacial maximum with implications for the melting history of the Laurentide ice sheet. Quat. Sci. Rev. 26, 920–940.

Simms, A.R., DeWitt, R., Rodriguez, A.B., Lambeck, K., Anderson, J.B., 2009. Revisiting marine isotope stage 3 and 5a (MIS3-5a) sea levels within the northwestern Gulf of Mexico. Glob. Planet. Change 66 (1–2), 100111. http://dx.doi.org/10.1016/j.gloplacha.2008.03.014.

Waelbroeck, C., Labeyrie, L., Michel, E., Duplessy, J.C., McManus, J.F., Lambeck, K., Balbon, E., Labracherie, M., 2002. Sea-level and deep water temperature changes derived from benthic foraminifera isotopic records. Quat. Sci. Rev. 21 (1–3), 295–305.

Wang, Y., Li, G., Zhang, W., Dong, P., 2014. Sedimentary environment and formation mechanism of the mud deposit in the central South Yellow Sea during the past 40kyr. Mar. Geol. 347, 123–135.

Wolstencroft, M., Shen, Z., Trnqvist, T.E., Milne, G.A., Kulp, M., 2014. Understanding subsidence in the Mississippi Delta region due to sediment, ice, and ocean loading: insights from geophysical modeling. J. Geophys. Res. Solid Earth 119, 38383856. http://dx.doi.org/10.1002/2013JB010928.

Yokoyama, Y., Lambeck, K., De Deckker, P., 2000. Timing of the last glacial maximum from observed sea-level minima, 406 (August), 1998–2001.